



Convergence of fracture process zone size in cohesive zone modeling [☆]



Kyungsu Ha, Hyunil Baek, Kyoungsoo Park ^{*}

Department of Civil and Environmental Engineering, Yonsei University, 50 Yonsei-ro Seodaemun-gu, Seoul 120-749, Republic of Korea

ARTICLE INFO

Article history:

Received 12 January 2015

Received in revised form 5 March 2015

Accepted 25 March 2015

Available online 31 March 2015

Keywords:

Fracture process zone
Cohesive zone model
Characteristic length
Nondimensional analysis

ABSTRACT

Nonlinear fracture process zone is associated with various material failure mechanisms, and thus its size estimation is of fundamental issues in understanding material failure behaviors. Then, the size of the fracture process zone is computationally estimated by utilizing a cohesive zone modeling approach. Geometrically similar single edge notched bending and compact tension configurations are employed with various combinations of the fracture energy, cohesive strength and elastic modulus, which lead to 91 cases. The computational results demonstrate the consistency and convergence of the fracture process zone size according to the change of the material properties and the increase of structural sizes. Additionally, the fracture process zone size is nondimensionalized through using a characteristic length. The nondimensionalized results illustrate the independence of material properties and structural geometries according to the increase of structural sizes. Therefore, the fracture process zone size in the cohesive zone model can be considered as an intrinsic material property.

© 2015 Elsevier Inc. All rights reserved.

1. Introduction

The estimation of fracture process zone is of fundamental issues in understanding nonlinear material failure behaviors. The fracture process zone is generally resulted from various mechanisms such as void nucleation, intergranular fracture, crack shielding due to micro-cracks, crack deflection, aggregate bridging, crack blunting, etc. Then, the size of the fracture process zone was analytically approximated in conjunction with linear elastic fracture mechanics, as summarized in [Table 1](#). Under the assumption of a constant stress redistribution ahead of a crack tip, a plastic zone size was evaluated by satisfying an equilibrium condition [\[1\]](#) or relating stress intensity factors from remote tension to closure stresses at a crack tip [\[2,3\]](#). Hillerborg et al. [\[4\]](#) addressed the effects of a critical length on concrete fracture behavior. In order to account for fracture of a progressively softening material like concrete, Bazant and Planas [\[5\]](#) employed a parabolic shape with degree n for stress distribution ahead of a crack tip. Hui et al. [\[6\]](#) estimated the cohesive zone length for a soft elastic solid by equating a stress field to a characteristic chain fracture stress. Note that although various approximation approaches are employed for the estimation of the fracture process zone size, all the estimated sizes are proportional to a characteristic size, defined as

[☆] This article belongs to the Special Issue: ASPEC 2013 – 2013 International Applied Science and Precision Engineering Conference, October 2013 NanTou, Taiwan.

^{*} Corresponding author. Tel.: +82 2 2123 5806.

E-mail address: k-park@yonsei.ac.kr (K. Park).

Table 1
Analytical approximation of the fracture process zone size.

Fracture process zone	References
$\frac{1}{\pi}EG_F/\sigma_{\max}$	Irwin [1]
$\frac{8}{3\pi}EG_F/\sigma_{\max}$	Barenblatt [2] and Dugdale [3]
EG_F/σ_{\max}	Hillerborg et al. [4]
$\frac{n+1}{\pi}EG_F/\sigma_{\max}$	Bazant and Planas [5]
$\frac{2}{3\pi}EG_F/\sigma_{\max}$	Hui et al. [6]

$$\ell_{ch} = \frac{EG_F}{\sigma_{\max}^2}, \tag{1}$$

where E , G_F and σ_{\max} are the elastic modulus, the fracture energy and the cohesive strength, respectively.

Alternatively, the fracture process zone was measured by utilizing various experimental techniques. For example, dye penetration was used to estimate the position and shape of a crack front [7,8]. Acoustic emission waves resulted from microcracking were detected by acoustic sensors, and related to the formation of the fracture process zone [9,10]. Additionally, a digital image correlation technique was employed to investigate the size and width of the fracture process zone and extract corresponding fracture parameters [11–13]. Note that the measured fracture process zone size depends on specimen geometry, structural sizes and material properties. Furthermore, it is generally different from the analytically estimated fracture process zone size listed in Table 1.

In this context, the fracture process zone size is computationally estimated by utilizing a cohesive zone modeling approach. The present study demonstrates the consistency and convergence of the fracture process zone size in the cohesive zone model, and thus the process zone size can be considered as an intrinsic material property. The effects of material properties and structural sizes on the fracture process zone are also addressed. The remainder of the paper is organized as follows. Section 2 presents the basic concept and finite element formulation of a cohesive zone modeling for crack growth simulation. Then, the fracture process zone in the cohesive zone model is defined and estimated in Section 3. In Section 4, computational results of single edge notched bending and compact tension test are provided with various combinations of material properties and structural sizes. Finally, the key findings are summarized in Section 5.

2. Cohesive zone modeling

Nonlinear fracture process zone is approximated by utilizing the concept of a cohesive zone model [2,3]. The cohesive zone model defines a traction–separation relationship in order to account for progressive damage and fracture mechanisms along fracture surface. For example, Barenblatt [2] and Dugdale [3] assumed a constant stress distribution for elastic–plastic fracture, while Hillerborg et al. [4] utilized a linear softening model for crack growth analysis of concrete. Further indepth reviews on traction–separation relations can be found in literature (e.g., [14]).

In the standard finite element method, the cohesive zone model is generally implemented by introducing cohesive surface elements. Prior to computational simulation, cohesive surface elements are inserted between continuum elements within a potential crack path, which leads to an *intrinsic cohesive zone modeling* approach. The intrinsic cohesive zone modeling approach has been widely utilized to investigate various failure behaviors such as quasi-brittle materials [15,16], adhesive bond joints [17,18], composite materials [19,20], etc. Alternatively, the cohesive zone model can be represented by other computational approaches such as extrinsic cohesive zone models [21–23], generalized/extended finite element methods [24], meshless methods [25], virtual internal bond models [26,27], peri-dynamics [28], etc. Note that the intrinsic cohesive zone model approach is the choice of the present study.

The finite element formulation of the intrinsic cohesive zone model is obtained from the principle of virtual work. The virtual work done by the external traction (\mathbf{T}_{ext}) on boundary (Γ) is equal to the summation of the virtual strain energy in domain (Ω) and the virtual cohesive fracture energy on fracture surface (Γ_c)

$$\int_{\Omega} \delta\epsilon : \boldsymbol{\sigma} dV + \int_{\Gamma_c} \delta\Delta \cdot \mathbf{T}_c dS = \int_{\Gamma} \delta\mathbf{u} \cdot \mathbf{T}_{ext} dS, \tag{2}$$

where $\delta\epsilon$ and $\delta\mathbf{u}$ are the virtual strain and the virtual displacement, respectively, and $\boldsymbol{\sigma}$ is the Cauchy stress tensor. The virtual cohesive fracture energy is obtained from the dot product of the virtual cohesive separation ($\delta\Delta$) and the cohesive traction (\mathbf{T}_c) where the cohesive traction–separation relationship is embedded in cohesive surface elements. Then, the internal force vector (\mathbf{f}_{coh}) and the tangent matrix (\mathbf{K}_{coh}) of cohesive surface elements are given as

$$\mathbf{f}_{coh} = \int_{\Gamma_c} \mathbf{B}_c^T \mathbf{T}_c dS, \tag{3}$$

and

$$\mathbf{K}_{coh} = \int_{\Gamma_c} \mathbf{B}_c^T \frac{\partial \mathbf{T}_c}{\partial \Delta} \mathbf{B}_c dS, \tag{4}$$

respectively, where a matrix (\mathbf{B}_c) provides the relationship between a global nodal displacement ($\bar{\mathbf{u}}$) and the local separation (Δ), i.e. $\Delta = \mathbf{B}_c \bar{\mathbf{u}}$ [29].

For the traction–separation relationship of the cohesive zone model, a linear softening model by Camanho et al. [30] is employed. Then, a state of separation is defined in conjunction with an effective separation ($\bar{\Delta}$), i.e.

$$\bar{\Delta} = \sqrt{\Delta_n^2 + \Delta_t^2}, \tag{5}$$

where Δ_n and Δ_t are normal and tangential separations, respectively. When an effective separation is smaller than a critical separation ($\bar{\delta}_{cr}$), the cohesive traction linearly increases to the cohesive strength (σ_{max}) according to the increase of separation

$$\mathbf{T}_c = K_p \Delta, \tag{6}$$

where a penalty stiffness (K_p) is the ratio of the cohesive strength to the critical separation, i.e. $K_p = \sigma_{max} / \bar{\delta}_{cr}$. If an effective separation is in between a critical separation ($\bar{\delta}_{cr}$) and a complete failure separation ($\bar{\delta}_f$), a damage variable (d) is introduced

$$d = \frac{\bar{\Delta} - \bar{\delta}_{cr}}{\bar{\Delta}(1 - \bar{\delta}_{cr} / \bar{\delta}_f)}, \tag{7}$$

for a linear softening. Note that the damage variable is initially zero, and monotonically increases to one with the increase of the effective separation. Then, the cohesive traction vector is given as

$$\mathbf{T}_c = (1 - d)K_p \Delta. \tag{8}$$

Finally, when the effective separation is greater than the complete failure separation, the cohesive traction is set to zero. The complete failure separation is evaluated by equating the fracture energy (G_F) to the area under the traction–separation relation, i.e. $\bar{\delta}_f = 2G_F / \sigma_{max}$.

3. Estimation of fracture process zone

The fracture process zone in the cohesive zone model is estimated through defining four states of cohesive separations: elastic stage, onset of fracture, progressive failure and complete failure (see Fig. 1). Before a crack initiation, the state of separation is considered as an elastic stage. At this stage, the separation is in between zero and the critical separation. When the separation is the critical separation, the cohesive traction reaches the cohesive strength, which corresponds to the onset of fracture. Then, the progressive damage and/or nonlinear fracture process along fracture surface is expected while a separation increases up to the complete failure separation. If separation is greater than the complete failure separation, no cohesive resistance exits along fracture surface. Therefore, the fracture process zone in the cohesive zone model is defined as the region for the progressive damage and/or nonlinear fracture process, which corresponds to the length between a position of the critical separation and a position of the complete failure separation along the fracture surface.

Then, the fracture process zone size is evaluated for a single edge notched bending test, as an example. The geometry and sizes of a single edge notched bending test are shown in Fig. 2. Three specimen sizes are employed with the widths (W) of 150, 500 and 6000 mm. The span (S) and the initial notch length (a_0) are $4W$ and $W/3$, respectively, with the thickness of 80 mm. The fracture energy and the cohesive strength are arbitrarily selected as 200 N/m and 6 MPa, respectively, with the elastic modulus of 30 GPa and the Poisson’s ratio of 0.2. Then, the applied load and the fracture process zone size are

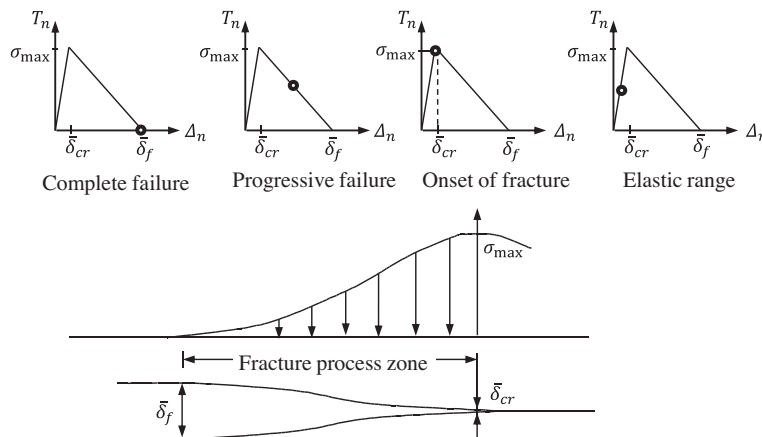


Fig. 1. Schematics of fracture process zone in the cohesive model.

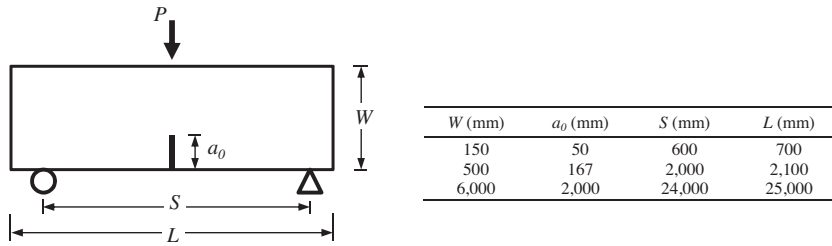


Fig. 2. Geometry and sizes of a single edge notched bending test.

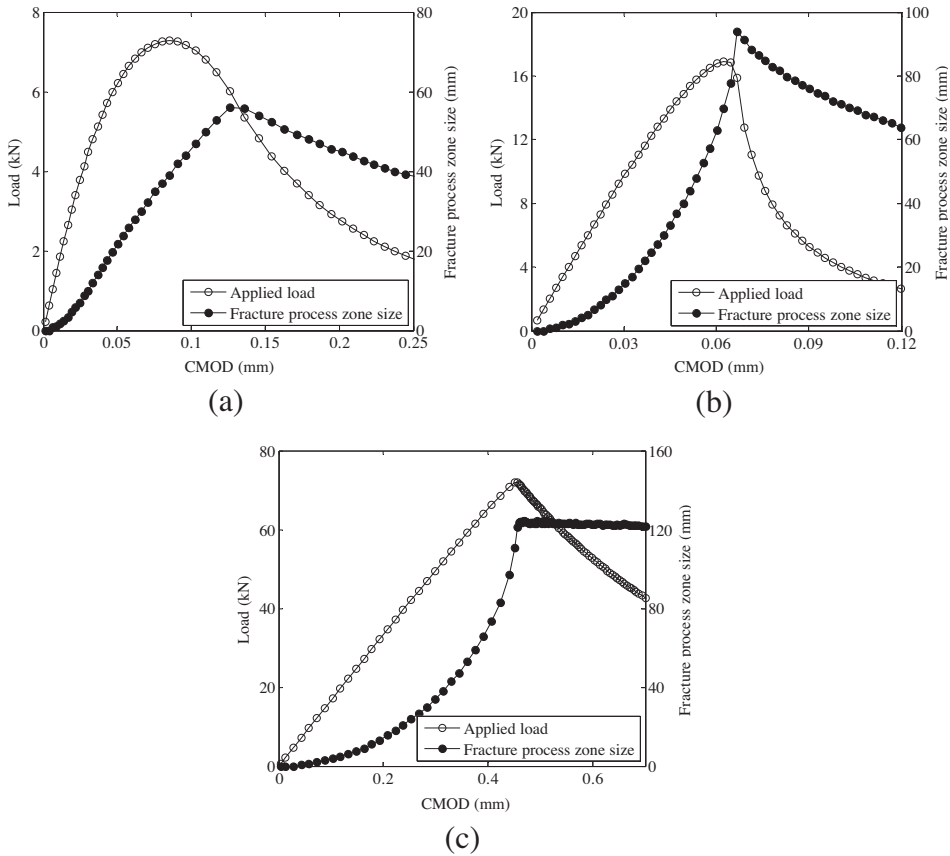


Fig. 3. Load and fracture process zone size with respect to CMOD for (a) $W = 150$ mm, (b) $W = 500$ mm and (c) $W = 6000$ mm.

plotted with respect to the crack mouth opening displacement (CMOD), as shown in Fig. 3. When the load is applied to the specimen, the size of the fracture process zone initially increases from an initial notch. For the specimen width of 150 mm (Fig. 3(a)), the applied load reaches maximum, and then the maximum process zone size is observed. After reaching the maximum process zone size, its size decreases to zero while a crack tip reaches to the boundary of a specimen. For the intermediate size ($W = 500$ mm), the maximum size of the fracture process zone is obtained right after the maximum load shown in Fig. 3(b), because the boundary effect decreases according to the increase of the specimen size. Note that if the structural size is large enough (e.g. $W = 6000$ mm), the size of the process zone remains almost constant after the load reaches a maximum value (Fig. 3(c)). Then, in this study, the maximum value of the fracture process zone size during computational simulation is selected as the fracture process zone size in the cohesive zone model (ℓ_{CZM}).

4. Computational results

The fracture process zone in the cohesive zone model is evaluated according to the changes of material properties and structural sizes. Two test configurations are employed, i.e. single edge notched bending and compact tension specimens,

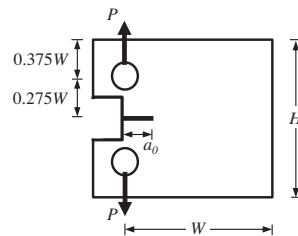


Fig. 4. Geometry of a compact tension test.

as illustrated in Figs. 2 and 4. Then, the non-dimensional analysis is performed on the basis of 56 cases of single edge notched bending tests and 35 cases of compact tension tests.

The crack propagation of single edge notched bending and compact tension specimens are simulated by utilizing a commercial finite element software, i.e. Abaqus [31]. The domain is discretized into bilinear quadrilateral elements while the cohesive crack is represented by inserting cohesive surface elements along a potential crack path. The positions of the critical separation and the complete failure separation are obtained by interpolating nodal displacement with shape functions.

4.1. Effects of material properties

In order to investigate the effects of material properties on the fracture process zone size, the fracture energy (G_f), the cohesive strength (σ_{\max}) and the elastic modulus (E) are changed with the constant Poisson's ratio of 0.2. The dimensions and material properties of single edge notched bending and compact tension specimens are summarized in Tables 2–4. For the effects of the fracture energy, the fracture energy is arbitrarily selected as 100, 200 and 400 N/m while the other material properties are fixed, i.e. the cohesive strength of 6 MPa and the elastic modulus of 30 GPa. Then, the estimated sizes of the fracture process zone (ℓ_{CZM}) are 61.5, 118.5 and 230.0 mm for the single edge notched bending test (Table 3) and 57.3, 105.1 and 183.3 mm for the compact tension test (Table 4). The increase of the fracture energy results in the increase of the process zone size because the higher fracture energy provides more resistance for a given separation along fracture surface. Furthermore, when the fracture energy is doubled, the process zone size is almost doubled, which corresponds to the relations in the analytical fracture process zone size (Table 1).

For the effects of the elastic modulus, the elastic modulus is varied as 30, 60 and 120 GPa with the fixed fracture energy and the cohesive strength. The fracture energy is 200 N/m for the single edge notched bending test and 100 N/m for the compact tension test, while the cohesive strength is 6 MPa for both tests. The increase of the elastic modulus leads to the increases of the fracture process zone size, as shown in Tables 3 and 4. Note that the process zone size is almost doubled when the elastic modulus increases two times.

Finally, the cohesive strength is chosen as 3, 6 and 12 MPa with a constant elastic modulus ($E = 30$ GPa). The fracture energy of the single edge notched bending test is 200 N/m and of the compact tension is 100 N/m. The calculated results demonstrate that the fracture process zone decreases with respect to the increase of the cohesive strength (Tables 3 and 4). This is because more brittle failure is expected for the higher cohesive strength and because the higher cohesive strength leads to a complete failure at a smaller separation. Additionally, when the cohesive strength is doubled, the process zone size decreases approximately four times. Thus, one expects that the process zone size is inverse proportional to the square of the cohesive strength in the cohesive zone modeling. In summary, the fracture process zone size (ℓ_{CZM}) of the cohesive zone model is proportional to the characteristic length (ℓ_{ch}).

4.2. Effects of structural size

The effects of structural sizes on the fracture process zone are investigated through changing structural sizes with a constant ratio of structural dimensions, which leads to geometrically similar structures. For a single edge notched bending test, an initial notch to width ratio (a_0/W) is 1/3 while a span to depth ratio is 4 (S/W) with a unit thickness. Then, the width of a specimen ranges from 63 mm to 12,000 mm with 8 cases, as shown in Table 5. The fracture energy and the elastic modulus are 200 N/m and 30 GPa, respectively, and three cohesive strengths are tested in this example (e.g. $\sigma_{\max} = 3, 6$ and 12 MPa). For a compact tension test, the initial notch to width ratio (a_0/W) of 1/5 is employed with a unit thickness. The range of the specimen width is from 50 to 6000 mm (5 cases), as summarized in Table 6. Similarly, the cohesive strengths are 3, 6 and 12 MPa with the fracture energy of 100 N/m and the elastic modulus of 30 GPa.

The evaluated fracture process zone size is plotted with respect to the structural size (Fig. 5). With the increase of the structural size (W), the size of the process zone increases while the change of the process zone size decreases for both single edge notched bending and compact tension specimens. Such results demonstrate the convergence of the process zone size to a constant value. In addition, the increase of the cohesive strength results in the faster convergence of the process zone size

Table 2

Dimensions of single edge notched bending and compact tension tests.

Single edge notched bending				Compact tension		
W (mm)	a_0 (mm)	S (mm)	L (mm)	W (mm)	a_0 (mm)	H (mm)
3000	1000	12,000	1300	1000	200	1200

Table 3

Effects of material properties on the fracture process zone size for single edge notched bending specimens.

G_f (N/m)	E (GPa)	σ_{\max} (MPa)	ℓ_{CZM} (mm)
100	30	6	61.5
200			118.5
400			230.0
200	30	6	118.5
	60		229.2
	120		415.6
200	30	3	417.2
		6	118.5
		12	31.5

Table 4

Effects of material properties on the fracture process zone size for compact tension specimens.

G_f (N/m)	E (GPa)	σ_{\max} (MPa)	ℓ_{CZM} (mm)
100	30	6	57.3
200			105.1
400			183.3
100	30	6	57.3
	60		104.7
	120		181.9
100	30	3	182.8
		6	57.3
		12	15.6

Table 5

Dimensions of single edge notched bending specimens.

Width, W (mm)	Initial notch, a_0 (mm)	Span, S (mm)	Length, L (mm)
63	21	250	350
150	50	600	700
250	83	1000	1100
500	167	2000	2100
1000	333	4000	4100
3000	1000	12,000	13,000
6000	2000	24,000	25,000
12,000	4000	48,000	50,000

Table 6

Dimensions of compact tension specimens.

Width, W (mm)	Initial notch, a_0 (mm)	Height, H (mm)
50	10	60
100	20	120
200	40	240
1000	200	1200
6000	1200	7200

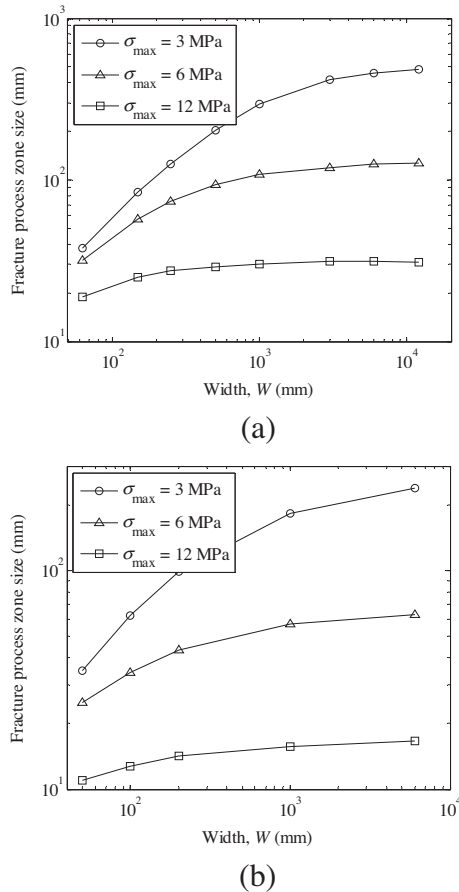


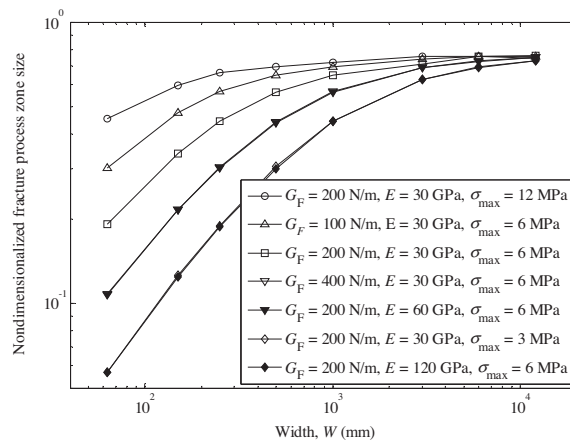
Fig. 5. Convergence of the fracture process zone size for (a) single edge notched bending and (b) compact tension specimens.

because the higher cohesive strength provides a smaller size of the fracture process zone, as discussed in the previous subsection.

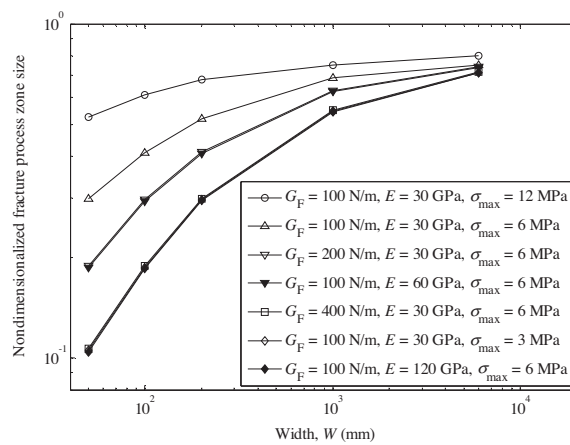
4.3. Non-dimensionalization of the fracture process zone

For non-dimensionalization of the fracture process zone, material properties listed in Tables 3 and 4 are utilized for the structural size provided in Tables 5 and 6, respectively. For the single edge notched bending test, 56 computational simulations are performed with 8 geometrically similar structures and 7 combinations of material properties. For the compact tension test, 35 computational simulations are performed with 5 geometrically similar structures and 7 combinations of material properties. The calculated fracture process zone size (ℓ_{CZM}) is divided by the characteristic size (ℓ_{ch}), which leads to a dimensionless characteristic factor.

The nondimensionalized fracture process zone is plotted according to the width of specimens, as shown in Fig. 6. The results demonstrate that the nondimensionalized fracture process zone size converges to a constant value while the width of specimens increases. The faster convergence of the nondimensionalized process zone size is observed when the calculated fracture process zone size is smaller, which corresponds to the smaller characteristic length (ℓ_{ch}). Additionally, the same characteristic length with different material property combinations can provide the same fracture process zone size. For example, the characteristic length with $G_f = 200$ N/m, $E = 30$ GPa and $\sigma_{max} = 3$ MPa is identical to the length with $G_f = 200$ N/m, $E = 120$ GPa and $\sigma_{max} = 6$ MPa, which is calculated as 666.7 mm. Such cases result in the same fracture process zone sizes in the cohesive zone model for given structural sizes, as illustrated in Fig. 6. Furthermore, the converged ratio of the fracture process zone in the cohesive zone model to the characteristic length is almost geometric independent because the converging value for the single edge notched bending test (0.73–0.76) is almost the same as for the compact tension tests (0.71–0.80).



(a)



(b)

Fig. 6. Non-dimensionalized results for (a) single edge notched bending and (b) compact tension specimens.

5. Conclusion

The size of nonlinear fracture process zone is computationally estimated in conjunction with the cohesive zone model. The single edge notched bending tests with 56 cases and the compact tension tests with 35 cases are considered. The calculated process zone size demonstrates similar trends with the analytical fracture process zone size. Material properties, which provide the same characteristic length, result in almost the same fracture process zone in the cohesive zone model. Additionally, when the fracture energy or the elastic modulus is doubled, the process zone size increases two times. If the cohesive strength decreases in half, the process zone size increases four times, which corresponds to the relations of the characteristic length. For geometrically similar structures, the process zone size converges to a constant value with respect to the increase of structural size. Furthermore, the nondimensionalized fracture process zone size also converges to a constant value for any combination of material properties. The converged value for the single edge notched bending test is almost the same as for the compact tension tests, and therefore, the evaluated fracture process zone size in the cohesive zone model can be considered as an intrinsic material property.

Acknowledgments

Dr. Park acknowledges support from the Korea Institute of Energy Technology Evaluation and Planning (KETEP) through Grant #20121620100040 and the National Research Foundation (NRF) of Korea through Grant # 2013M2B2A4041330. The information presented in this paper is the sole opinion of the authors and does not necessarily reflect the views of the sponsoring agencies.

References

- [1] G.R. Irwin, Plastic zone near a crack and fracture toughness, in: *Sagamore Research Conference Proceedings*, vol. 4, 1961.
- [2] G.I. Barenblatt, The formation of equilibrium cracks during brittle fracture: general ideas and hypotheses, axially symmetric cracks, *Appl. Math. Mech.* 23 (3) (1959) 622–636.
- [3] D.S. Dugdale, Yielding of steel sheets containing slits, *J. Mech. Phys. Solids* 8 (2) (1960) 100–104.
- [4] A. Hillerborg, M. Modeer, P.E. Petersson, Analysis of crack formation and crack growth in concrete by means of fracture mechanics and finite elements, *Cem. Concr. Res.* 6 (6) (1976) 773–781.
- [5] Z.P. Bazant, J. Planas, *Fracture and Size Effect in Concrete and other Quasibrittle Materials*, CRC Press, Boca Raton, 1998.
- [6] C.-Y. Hui, A. Jagota, S.J. Bennison, J.D. Londono, Crack blunting and the strength of soft elastic solids, *Proc. R. Soc. London A: Math. Phys. Eng. Sci.* 459 (2034) (2003) 1489–1516.
- [7] S.E. Swartz, C.G. Go, Validity of compliance calibration to cracked concrete beams in bending, *Exp. Mech.* 24 (2) (1984) 129–134.
- [8] S.E. Swartz, T.M.E. Refai, Influence of size effects on opening mode fracture parameters for precracked concrete beams in bending, in: S.P. Shah, S.E. Swartz (Eds.), *Fracture of Concrete and Rock*, Springer, New York, 1989, pp. 242–254.
- [9] H. Mihashi, N. Nomura, S. Niiseki, Influence of aggregate size on fracture process zone of concrete detected with three dimensional acoustic emission technique, *Cem. Concr. Res.* 21 (5) (1991) 737–744.
- [10] E.N. Landis, Micro–macro fracture relationships and acoustic emissions in concrete, *Constr. Build. Mater.* 13 (1–2) (1999) 65–72.
- [11] B. Shen, G.H. Paulino, Direct extraction of cohesive fracture properties from digital image correlation: a hybrid inverse technique, *Exp. Mech.* 51 (2) (2011) 143–163.
- [12] Ł. Skarżyński, E. Syroka, J. Tejchman, Measurements and calculations of the width of the fracture process zones on the surface of notched concrete beams, *Strain* 47 (2011), 1475–1305.
- [13] J.-C. Oh, H.-G. Kim, Inverse estimation of cohesive zone laws from experimentally measured displacements for the quasi-static mode I fracture of PMMA, *Eng. Fract. Mech.* 99 (2013) 118–131.
- [14] K. Park, G.H. Paulino, Cohesive zone model: a critical review of traction–separation relationships across fracture surface, *Appl. Mech. Rev.* 64 (6) (2013) 060802.
- [15] J.R. Roesler, G.H. Paulino, K. Park, C. Gaedicke, Concrete fracture prediction using bi-linear softening, *Cement Concr. Compos.* 29 (4) (2007) 300–312.
- [16] K. Park, G.H. Paulino, J.R. Roesler, Cohesive fracture modeling of functionally graded fiber reinforced concrete composite, *Cem. Concr. Res.* 40 (6) (2010) 956–965.
- [17] M. Alfano, F. Furguieue, A. Leonardi, C. Maletta, G.H. Paulino, Mode I fracture of adhesive joints using tailored cohesive zone models, *Int. J. Fract.* 157 (1–2) (2009) 193–204.
- [18] S. Akpinar, M.D. Aydin, A. Özel, A study on 3-D stress distributions in the bi-adhesively bonded T-joints, *Appl. Math. Model.* 37 (24) (2013) 10220–10230.
- [19] D. Ngo, K. Park, G.H. Paulino, Y. Huang, On the constitutive relation of materials with microstructure using the PPR potential-based cohesive model for interface interaction, *Eng. Fract. Mech.* 77 (7) (2010) 1153–1174.
- [20] A. Needleman, T.L. Borders, L.C. Brinson, V.M. Flores, L.S. Schadler, Effect of an interphase region on debonding of a CNT reinforced polymer composite, *Compos. Sci. Technol.* 70 (2010) 2207–2215.
- [21] G.T. Camacho, M. Ortiz, Computational modelling of impact damage in brittle materials, *Int. J. Solids Struct.* 33 (20–22) (1996) 2899–2938.
- [22] Z. Zhang, G.H. Paulino, W. Celes, Extrinsic cohesive modelling of dynamic fracture and microbranching instability in brittle materials, *Int. J. Numer. Methods Eng.* 72 (8) (2007) 893–923.
- [23] K. Park, G.H. Paulino, W. Celes, R. Espinha, Adaptive mesh refinement and coarsening for cohesive dynamic fracture, *Int. J. Numer. Methods Eng.* 92 (1) (2012) 1–35.
- [24] N. Moes, T. Belytschko, Extended finite element method for cohesive crack growth, *Eng. Fract. Mech.* 69 (7) (2002) 813–833.
- [25] Y. Dong, S. Wu, S.S. Xu, Y. Zhang, S. Fang, Analysis of concrete fracture using a novel cohesive crack method, *Appl. Math. Model.* 34 (12) (2010) 4219–4231.
- [26] H. Gao, P. Klein, Numerical simulation of crack growth in an isotropic solid with randomized internal cohesive bonds, *J. Mech. Phys. Solids* 46 (2) (1998) 187–218.
- [27] K. Park, G.H. Paulino, J.R. Roesler, Irregular internal pair-bond (VIPB) model for quasi-brittle materials, *J. Eng. Mech. – ASCE* 134 (10) (2008) 856–866.
- [28] Y.D. Ha, F. Bobaru, Studies of dynamic crack propagation and crack branching with peridynamics, *Int. J. Fract.* 162 (1–2) (2010) 229–244.
- [29] K. Park, G.H. Paulino, Computational implementation of the PPR potential-based cohesive model in ABAQUS: Educational perspective, *Eng. Fract. Mech.* 93 (2012) 239–262.
- [30] P.P. Camanho, C.G. Davila, M.F. De Moura, Numerical simulation of mixed-mode progressive delamination in composite materials, *J. Compos. Mater.* 37 (16) (2003) 1415–1438.
- [31] Abaqus, *Abaqus 6.13 Analysis User's Manual*, SIMULIA, Providence, IR, 2013.